



Thin current sheet in the substorm late growth phase: Modeling of THEMIS observations

X.-Z. Zhou,^{1,2} V. Angelopoulos,¹ A. Runov,¹ M. I. Sitnov,³ F. Coroniti,⁴ P. Pritchett,⁴ Z. Y. Pu,² Q.-G. Zong,^{2,5} J. P. McFadden,⁶ D. Larson,⁶ and K.-H. Glassmeier⁷

Received 29 September 2008; revised 8 January 2009; accepted 15 January 2009; published 31 March 2009.

[1] The structure of a thin current sheet prior to the expansion onset of a substorm event that occurred on 26 February 2008 is studied in the near-Earth magnetotail on the basis of Time History of Events and Macroscale Interactions During Substorms (THEMIS) observations. During this time interval, the ion distribution showed mushroom-shaped structures with clear nongyrotropic features, indicating that the warmer component of the ions was unmagnetized, which becomes possible only if the gyroradii of these ions are comparable with the current sheet thickness. By comparing the observations with the model proposed by Sitnov et al. (2003), which is a modification of the Harris (1962) model by considering the effect of the meandering ions in thin current sheets, we reconstruct the current sheet structure in the late growth phase of the substorm. Warmer ions, mostly following meandering orbits across the neutral sheet, are found to remarkably alter the current sheet profiles and therefore play an important role in the formation of the thin current sheet.

Citation: Zhou, X.-Z., et al. (2009), Thin current sheet in the substorm late growth phase: Modeling of THEMIS observations, *J. Geophys. Res.*, 114, A03223, doi:10.1029/2008JA013777.

1. Introduction

[2] The *Harris* [1962] equilibrium, based on a self-consistent solution of the Vlasov-Maxwell equations, has been widely accepted as the standard model of the current sheet. In the Harris theory, the particle distributions are assumed to be exponential functions of two exact invariants of motion, i.e., the total particle energy and the canonical momentum along the current direction, to obey the Vlasov equation. The distributions, in the form of a shifted Maxwellian, are then substituted into the Maxwell equations to obtain a hyperbolic tangent profile of the magnetic field in the current sheet. The current and plasma density in the Harris model have similar profiles monotonically decreasing with the distance from the neutral plane.

[3] However, many observations [e.g., *Sergeev et al.*, 1993; *Runov et al.*, 2003] revealed that the current sheet

could strongly differ from the Harris model, either having a bifurcated current density profile or embedded into a thicker plasma sheet, especially when the thickness of the current sheet becomes relatively small. Actually, the formation of a thin current sheet (TCS) is one of the most significant signatures in the near-Earth magnetotail during the late growth phase of substorms [e.g., *Baumjohann et al.*, 2007, and references therein]. The current sheet thickness can be as small as several hundred kilometers [e.g., *Mitchell et al.*, 1990; *Asano et al.*, 2004; *Runov et al.*, 2008], that is, on the order of the thermal ion gyroradius.

[4] The observed deviation from the standard Harris sheet, therefore, requires a modification of the Harris model. The distribution function may be modified, either by selecting a more complicated function of the energy and the canonical momentum along the current direction [e.g., *Schindler and Birn*, 2002], or by adding more invariants of motion into the system, such as the magnetic moment [*Francfort and Pellat*, 1976]. However, an additional problem is that the motions of ions and electrons in the thin current sheets are often decoupled: the electrons are still magnetized, while some of the ions follow the meandering figure-eight orbits [*Speiser*, 1965] across the neutral sheet. In this case, the conventional guiding center theory is no longer valid, which also invalidates all three of the traditional adiabatic invariants including the magnetic moment. Fortunately, as was suggested by *Sonnerup* [1971], there exists another adiabatic invariant, that is, the sheet invariant I_z which remains approximately constant of motion when the particle thermal gyroradius exceeds the curvature radius of the magnetic field [*Büchner and Zelenyi*, 1989].

¹Institute of Geophysics and Planetary Physics, University of California, Los Angeles, California, USA.

²School of Earth and Space Sciences, Peking University, Beijing, China.

³Johns Hopkins University Applied Physics Laboratory, Laurel, Maryland, USA.

⁴Department of Physics and Astronomy, University of California, Los Angeles, California, USA.

⁵Center for Atmospheric Research, University of Massachusetts, Lowell, Massachusetts, USA.

⁶Space Science Laboratory, University of California, Berkeley, California, USA.

⁷Institute for Geophysics and Extraterrestrial Physics, TU Braunschweig, Braunschweig, Germany.

[5] By taking into account the contribution of the sheet invariant I_z to the particle distribution functions, the standard Harris model can be modified [Sitnov *et al.*, 2003, 2004, 2006], hereinafter referred to as the SGS model, to describe the embedded or bifurcated features of the thin current sheet with the existence of the unmagnetized particles. Then the distribution functions could be substituted to the Ampère's equation and the quasi-neutrality equation, and the solution of these equations yields a self-consistent magnetic profile of the current sheets, which can deviate significantly from the standard hyperbolic tangent function.

[6] Another difference between the Harris model and the self-consistent SGS model is that the SGS model provides some anisotropy and nongyrotropy in the particle distribution functions, which arise from the coexistence of the gyrating (noncrossing) and meandering particles in the thin current sheet. Particles with the same energy but moving in different directions can experience distinct orbits and therefore have very different I_z values, which results in the asymmetry of the particle distribution in the velocity space.

[7] In this paper, we focus on the particle distributions observed by the Time History of Events and Macroscale Interactions During Substorms (THEMIS) constellation [Angelopoulos, 2008] in the current sheet during the late growth phase of a substorm event on 26 February 2008 [Angelopoulos *et al.*, 2008]. The ion distributions, observed by THEMIS P1 and P2, both contain two components, a gyrotropic colder component and a warmer one with many more duskward moving ions. These two components then compose a mushroom-shaped structure in the velocity space perpendicular to the magnetic field. With a minor modification to include these two ion components, the SGS model is used to fit the observed nongyrotropic ion distributions and to explain the role of the meandering ions in the thin current sheet.

2. Harris and SGS Models

[8] Before going to the detailed observations, we start with a brief review of the Harris [1962] model and its modifications, especially the SGS model.

[9] In order to better present the current sheet in the magnetotail, the coordinate system is defined as follows: the y and the z axes denote the current direction and the normal direction of the current sheet, respectively, and the x axis completes the orthogonal set. It should be noted that the magnetic field is mainly in the x direction.

[10] The key element of the Harris model is the assumption that the ion and electron distributions are taken as the functions of two integrals of motion, say, the particle energy $W_\alpha = m_\alpha v^2/2 + q_\alpha \phi$ and the y component of the canonical momentum $P_{y\alpha} = m_\alpha v_y + (q_\alpha/c)A_y$. Here the subscript α suggests the particle species (ions or electrons), while ϕ and A_y are the electric potential and the y component of the magnetic vector potential, respectively.

[11] For any given nonnegative combinations of these two invariants of motion, the distribution function would automatically satisfy the Vlasov equation. In the Harris model, the exponential function is selected, and the distribution function becomes

$$f_{0\alpha} \propto \exp[-(W_\alpha - v_{D\alpha} P_{y\alpha})/T_\alpha], \quad \alpha = e, i \quad (1)$$

where T_α and $v_{D\alpha}$ represent the temperature and the bulk flow speed for the species α , respectively. Moreover, the electric potential ϕ can be eliminated from the system by selecting a quasi-neutrality frame in which the condition $T_i/q_i v_{Di} = T_e/q_e v_{De} (=G)$ is satisfied. If the boundary conditions $B_{|z=0} = 0$ and $B_{|z \rightarrow \infty} = B_0$ are used, the Maxwell equations would yield a solution in the form of the magnetic field profile

$$B_x = B_0 \tanh(z/L) \quad (2)$$

where $L = 2cG/B_0$ is the characteristic thickness of the current sheet. In addition to the well-known hyperbolic tangent profile of the magnetic field, the profiles of the plasma density and the current density can be also obtained, both proportional to $\cosh^{-2}(z/L)$, with their maxima appearing at the center of the current sheet along with the magnetic field minimum.

[12] The Harris model is by default a purely antiparallel model with the magnetic field solely in the x direction, although in many studies, a weak magnetic component B_z is superposed into the background magnetic field [e.g., Lembège and Pellat, 1982; Birn and Priest, 2007]. It should be noted that the introduction of the B_z component would provide an x -dependent term $q_\alpha B_z x$ into the canonical momentum P_y , which appears to significantly complicate the case. However, as was suggested by Schindler [1972], the P_y dependence on x values can be neglected in the zeroth-order approximation, if the B_z component is much smaller than the lobe magnetic field B_0 .

[13] It should be also noted that equation (1), the distribution function for species α , can be rewritten as the function of the velocity components, that is:

$$f_{0\alpha} \propto \exp\left(\frac{A_y}{cG} + \frac{m_\alpha v_{D\alpha}^2}{2T_\alpha}\right) \cdot e^{-\frac{m_\alpha}{2T_\alpha}[v_x^2 + v_z^2 + (v_y - v_{D\alpha})^2]} \quad (3)$$

which suggests that the particle distributions in the Harris sheet are always Maxwellian, with a location-independent velocity shift v_D in the y direction. The velocity shift can be understood as the diamagnetic drift, which comes from the density gradient pointing toward the center of the Harris sheet. In the northern/southern half of the current sheet, for instance, the duskward moving ions have their orbits mostly located in the more populated region southward/northward of the satellite, and therefore leading to the asymmetry with more fluxes in the duskward direction, which corresponds to the net duskward drift velocity v_D .

[14] The Harris model, although widely used as the standard current sheet model, does not always agree with the observations. The shifted Maxwellian distribution in the Harris sheet is rather simple in comparison with the complicated observational data [e.g., Hoshino *et al.*, 1998]. Furthermore, the observed current density profile in the current sheet can be either bifurcated [e.g., Asano *et al.*, 2005], or embedded into a broader current and plasma density layer [e.g., Sergeev *et al.*, 1993], which deviates from the hyperbolic profile in the Harris model. Therefore, a more generalized model is required, to provide more flexibility and to reproduce the more complicated features of the current sheet.

[15] One of the approaches to generalize the Harris model is to express the distribution function by adopting more general combinations of W_α and $P_{y\alpha}$, instead of the linear combination used in equation (1). A series of these models have been developed [e.g., *Channell*, 1976; *Schindler and Birn*, 2002; *Mottez*, 2003; *Birn et al.*, 2004; *Génot et al.*, 2005; *Camporeale and Lapenta*, 2005], with the distribution functions assumed to be

$$f_{0\alpha} \propto \exp[-W_\alpha/T_\alpha] \cdot g_\alpha(P_{y\alpha}), \quad \alpha = e, i \quad (4)$$

where $g_\alpha(P_{y\alpha})$, in general, can be any nonnegative function. Once the function of g_α (and therefore the distribution function $f_{0\alpha}$) is specified, the profiles of the magnetic field, the plasma density and the current density can be obtained, by solving the Maxwell equations either numerically or analytically.

[16] These models, by selecting different g_α functions, are able to reproduce many of the observed structures, such as the embedded [*Schindler and Birn*, 2002; *Birn et al.*, 2004] and the bifurcated [*Birn et al.*, 2004; *Camporeale and Lapenta*, 2005] current sheets. For example, by selecting

$$g_i(P_y) = g_e(-P_y) = e^{-P_y} [1 - 0.5 \tanh(20P_y)] \quad (5)$$

in equation (4), as was proposed by *Schindler and Birn* [2002] and *Birn et al.* [2004], the self-consistent solution of the model has a current density profile with strong enhancement in the center of the current sheet, which means that the modeled current sheet is an embedded one.

[17] However, the equilibria were often achieved at the expense of rather uneven distributions with significant stability issues. For instance, the modeled thin current sheet (with a thickness of less than twice the thermal ion gyro-radius) suggested by *Birn et al.* [2004] was found to collapse to a Harris-like sheet within one gyroperiod [*Camporeale and Lapenta*, 2005] because of the excitation of the lower hybrid drift instability (LHDI). Moreover, a probably more fundamental problem arises, according to the view of *Sitnov et al.* [2006], from the selection of the specific combination of the two invariants. Any artificial choices of the combination, as long as they are nonnegative, can always satisfy the Vlasov equations and therefore correspond to a self-consistent solution; however, the physical significance of these arbitrary choices is questionable.

[18] Another way to modify the Harris model is to extend the sets of integrals of motion, by introducing the so-called sheet invariant [e.g., *Sonnerup*, 1971; *Francfort and Pellat*, 1976; *Büchner and Zelenyi*, 1989; *Zelenyi et al.*, 2000], which arises from the particle dynamics [e.g., *Speiser*, 1965] near the neutral sheet.

[19] As we know, a significant portion of the particles would not experience Larmor motion, but follow the meandering orbits across the neutral sheet, especially when the current sheet thickness L becomes comparable to the thermal ion gyroradius ρ . Therefore, the particle dynamics does not obey the conventional guiding center theory, but instead becomes approximately adiabatic or “quasi-adiabatic” as long as the condition

$$|B_z|/B_0 \ll (\rho/L)^{1/2} \quad (6)$$

is satisfied [*Büchner and Zelenyi*, 1989; *Kropotkin et al.*, 1997], and the magnetic field becomes slightly curved. In this case, a special integral of motion can be introduced [*Sonnerup*, 1971], that is, the sheet invariant

$$I_z^{(\alpha)} = \frac{1}{2\pi} \oint P_{z\alpha} dz \quad (7)$$

where $P_{z\alpha}$ is the z component of the canonical momentum, and the integral sign \oint indicates integration over the entire period of the particle oscillatory motion in the z direction.

[20] In the SGS model, the sheet invariant $I_z^{(\alpha)}$ is linearly combined with the other two invariants of motion (W_α and $P_{y\alpha}$) in the distribution functions [*Sitnov et al.*, 2003, 2004, 2006], and the form becomes

$$f_{0\alpha} \propto \exp \left[-\frac{W_\alpha}{T_{\parallel\alpha}} + \frac{v_{D\alpha} P_{y\alpha}}{T_{\parallel\alpha}} + \left(\frac{\omega_{0\alpha}}{2T_{\parallel\alpha}} - \frac{\omega_{0\alpha}}{2T_{\perp\alpha}} \right) I_z^{(\alpha)} \right] \quad (8)$$

where $T_{\parallel\alpha}$, $T_{\perp\alpha}$ and $\omega_{0\alpha} = eB_0/m_\alpha c$ are the parallel temperature, the perpendicular temperature and the cyclotron frequency outside the sheet for the species α , respectively. In the limit of $T_{\parallel} = T_{\perp}$, it is clear that the SGS distribution function (8) becomes exactly the same with the standard Harris distribution (1) with no dependence on $I_z^{(\alpha)}$. For more general cases with $T_{\parallel} \neq T_{\perp}$, the Ampère's equation and the quasi-neutrality equation can be solved numerically, by iterations starting from the Harris solution and at each step updating the current sheet profiles until convergence is reached.

[21] One of the key features of the SGS model is the presence of the non-Maxwellian ion distributions with some degree of nongyrotropy, which arises directly from the I_z dependence of the distribution function. For relatively thicker current sheets, most of the ions can still gyrate around the magnetic field, and the sheet invariant I_z degenerates to the magnetic moment. Therefore, the shifted Maxwellian is still a good approximation to describe the ion distribution functions. When the current sheet thickness becomes comparable to the thermal ion gyroradius, however, the rotational symmetry of these ions to the magnetic field is lost, and the contribution of the orbit-dependent value of I_z to the distribution function becomes significant.

[22] Figure 1, adapted from *Sonnerup* [1971] and *Zhou et al.* [2007], describes the dependence of the sheet invariant I_z on the configuration of the particle trajectory, which is quantified by the trajectory form parameter k , defined by *Sonnerup* [1971] as $k = [(1/2)(1 - P_y/mv_\perp)]^{1/2}$. For various k values, the configuration of the particle orbit is also shown in the top part of Figure 1. In general, the value of I_z is relatively small if the particle is gyrating around the magnetic field away from the neutral sheet ($k > 1$), or if the particle is following the meandering orbit across the neutral sheet drifting in the electric current direction (duskward for ions in the tail current sheet) at a speed comparable to the particle velocity ($0 \leq k \ll 1$). The I_z value is larger, on the other hand, if the value of k is slightly smaller than 1 (see the shaded area of Figure 1), which means the particle is meandering either in the opposite

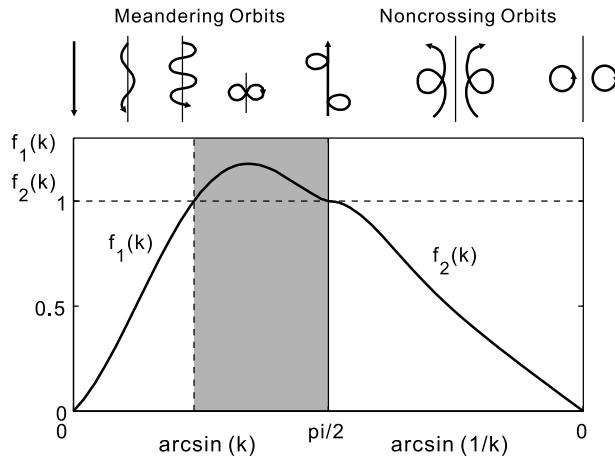


Figure 1. Dependence of the sheet invariant I_z on the form parameter k within the current sheet, adapted from *Sonnerup* [1971] and *Zhou et al.* [2007]. The sheet invariant I_z is proportional to $f_1(k)$ for the meandering orbit (left part, i.e., $k \leq 1$) and proportional to $f_2(k)$ for the noncrossing orbit (right part, i.e., $k > 1$). The shaded area corresponds to the k range with relatively larger I_z values. Also shown at the top is the nature of the orbit for various k values.

direction of the electric current (dawnward for ions), or at a relatively small speed in the current direction.

[23] Therefore, in the very center of the SGS current sheet where meandering particles dominate, if I_z contributes negatively to the ion distribution function (8), that is, $T_{\parallel i} > T_{\perp i}$, the phase space densities for ions meandering toward the dusk (with smaller I_z values) will be greater than those for dawnward meandering ions (with higher I_z values), suggesting an enhancement of the electric current

at the center of the current sheet, that is, the embedded current sheet. Similarly, the bifurcated current sheet can be reproduced in the SGS model, with a current minimum at the center of the current sheet, if I_z contributes positively to the ion distribution function, i.e., $T_{\parallel i} < T_{\perp i}$. In this case, as was shown by *Sitnov et al.* [2006, Figure 3f], a mushroom-shaped distribution can be found near the current maximum region, and the mushroom cap corresponds to those particles meandering across the neutral sheet (with higher I_z values than those noncrossing particles).

[24] Note that the effect of different plasma anisotropy values on the current sheet structure (embedding when $T_{\parallel i} > T_{\perp i}$ and bifurcation when $T_{\parallel i} < T_{\perp i}$), based on the SGS model, agrees well with the pioneering fluid-based study made by *Cowley* [1978]. The usage of the sheet invariant I_z in the distribution function (8), as the generation of the Harris model, also provides a kinetic and nongyrotopropic analog of the *Cowley* [1978] theory.

[25] Unlike the current sheet model proposed by *Birn et al.* [2004], the SGS current sheet is rather stable and the LHDI instability develops only slightly, as was confirmed by particle simulations performed by *Sitnov et al.* [2006]. The much more stable structure of the SGS model, according to the view of *Sitnov et al.* [2006], confirms that the introduction of an additional invariant of motion I_z is robust and likely more physical, compared to the a priori selection of a specific distribution function, as was done, e.g., in the *Birn et al.* [2004] model.

[26] With the pictures of the SGS model kept in mind, we turn to the THEMIS observations in the magnetotail current sheet. With special emphasis on the ion distributions, the 26 February 2008 substorm event is studied in the next section, by using the data from Electro-Static Analyzer (ESA) instrument [*McFadden et al.*, 2008] and Fluxgate Magnetometer (FGM) instrument [*Auster et al.*, 2008].

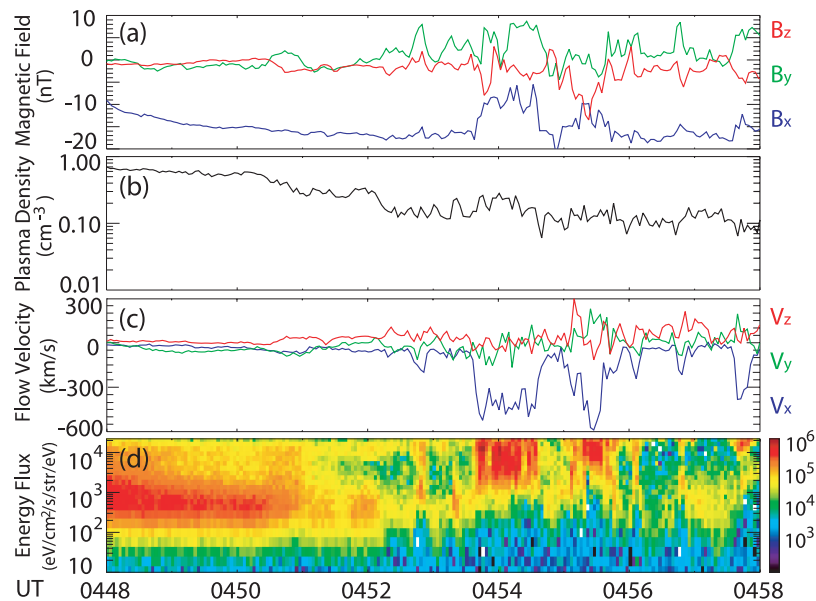


Figure 2. Overview of the magnetic field and the plasma data for 10 min, observed by THEMIS P1 satellite during the substorm event of 26 February 2008. (a) The three components of the magnetic field in the GSM coordinate system. (b) The plasma density. (c) The ion bulk flow velocity, also in the GSM coordinates. (d) The energy spectra of 0.01- to 20-keV ions.

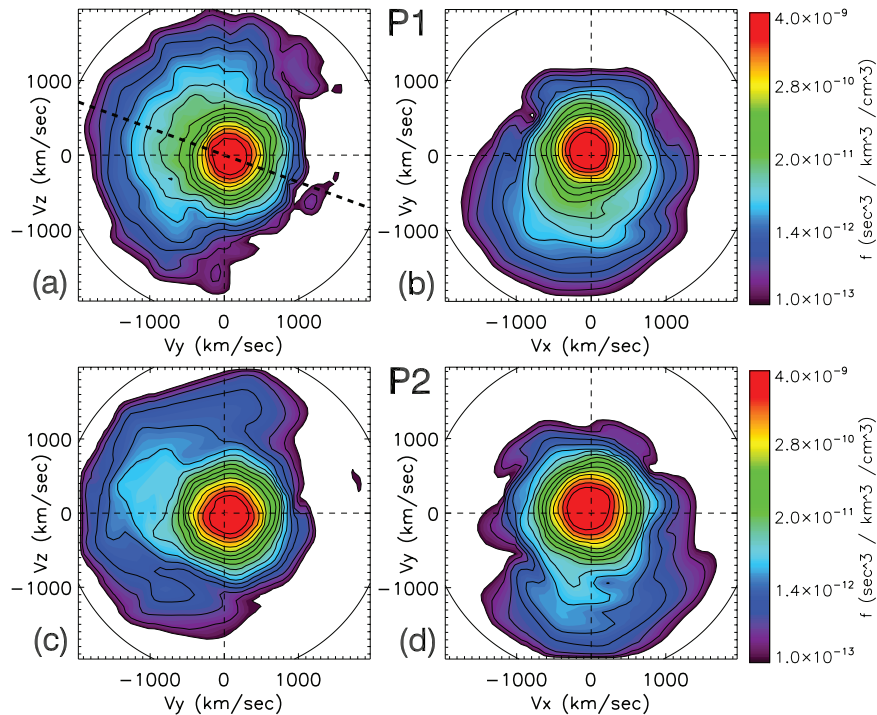


Figure 3. THEMIS P1 and P2 observations of the ion distribution functions in the despun spacecraft coordinates (+ x is Earthward, + y is dawnward, and + z is southward) during the substorm event of 26 February 2008. (a and b) The cuts of the three-dimensional ion distribution in the yz and the xy plane, respectively, observed by P1 during 0450:17–0450:26 UT. The thick dashed line in the yz plane suggests an axis of symmetry of the ion distribution, which has an angle of 20° with the y axis. (c and d) The yz and xy cuts of the ion distribution, observed by P2 during 0445:50–0445:59 UT.

Further details of this event are given by *Angelopoulos et al.* [2008].

3. Observations

[27] Figure 2 provides a 10-min overview of the event observed by the THEMIS P1 satellite, which was located in the magnetotail with $X_{GSM} = -21.5 R_E$ at 0450 UT. Shown are the magnetic field (Figure 2a), the plasma density (Figure 2b), the ion bulk flow velocity (Figure 2c), and the ion energy spectra (Figure 2d).

[28] It can be clearly seen that the observed magnetic field was predominantly in the $-x$ direction, which means that the P1 satellite was located south of the neutral sheet. Before the onset of the fast tailward flows, the decreasing plasma density and the increasing magnetic magnitude further suggest the decreasing of the current sheet thickness, as can be expected at substorm growth phase. Despite the current sheet thinning, the relatively high plasma density suggests that P1 remained within the plasma sheet.

[29] Two ion components were observed at before the substorm expansion onset: a 500-eV (colder) component and a 10-keV (warmer) one, as was suggested by *Angelopoulos et al.* [2008] and can be also seen in Figure 2d. Here the observed ions are assumed to be protons since the THEMIS/ESA instrument cannot distinguish different ion species. Figures 3a and 3b provide a better view of these two components, which are the ion velocity distributions observed at P1 during 0450:17–0450:26 UT, in the yz and the xy plane of the spacecraft coordinates, respectively. To

minimize statistical fluctuations, the distributions are averaged over 3 spin periods.

[30] Since the magnetic field was predominately in the $-x$ direction, Figure 3a corresponds to the distribution perpendicular to the magnetic field. The most pronounced feature here is the strong nongyrotropy of the warmer component of the ions, with a higher flux of duskward moving ions than the dawnward ones. The colder component, on the other hand, deviates little from the gyrotropy besides a minor shift dawnward. These two components, therefore, compose a mushroom-shaped structure in the velocity space. Figure 3b, showing the ion distribution in the plane containing the magnetic field, also clearly exhibits the nongyrotropic features of the warmer ion component.

[31] Figures 3c and 3d show the yz and xy cuts of the ion distributions observed by P2, which was over $4 R_E$ closer to the Earth, during 0445:50–0445:59 UT. Despite a lower resolution since P2 was not in burst mode, the ion distributions have very similar features, with an isotropic colder component and a warmer duskward moving component. It should be noted that the magnetic reconnection site was located somewhere between P1 and P2, as was suggested by *Angelopoulos et al.* [2008], which makes it even more important to study the origin of these distributions and the structure of the non-Harris current sheet.

4. Current Sheet Reconstruction

[32] The SGS model, as the self-consistent model to study the thin current sheet, is used in this section to fit the

observations. On the basis of the two-component features of the observed distribution, the model is slightly modified with the ion distribution function of

$$f_{0i} = \frac{N_w \pi^{-\frac{3}{2}} \delta_{iw}}{v_{T\perp iw}^2 v_{T\parallel iw}} \exp \left[\frac{v_{Diw} P_y - W}{T_{\parallel iw}} + \frac{1}{2} \left(\frac{\omega_{0i}}{T_{\parallel iw}} - \frac{\omega_{0i}}{T_{\perp iw}} \right) I_z \right] + N_c \pi^{-\frac{3}{2}} v_{Tc}^{-3} \exp \left[(v_{Dic} P_y - W) / T_{ic} \right] \quad (9)$$

where the subscripts w and c correspond to the warmer and the colder components of the ions, respectively. Here v_T and N are the thermal velocity and the nominal plasma density, with $\delta_{iw} = \exp[-(v_{Diw}^2/v_{T\parallel iw}^2)(T_{\perp iw}/T_{\parallel iw} - 1)]$. As can be directly seen from equation (9), the assumed distribution function is simply a weighted superposition of two types of distributions: a colder shifted Maxwellian distribution and a warmer SGS model-type distribution with the contribution of the sheet invariant I_z .

[33] The electron distribution function, on the other hand, is assumed to be

$$f_{0e} = N_w \pi^{-\frac{3}{2}} v_{Tew}^{-3} \exp[(v_{Dew} P_y - W) / T_{ew}] + N_c \pi^{-\frac{3}{2}} v_{Tec}^{-3} \exp[(v_{Dec} P_y - W) / T_{ec}] \quad (10)$$

which is a superposition of two shifted Maxwellian distributions. Here, for simplicity, we do not consider the contribution of the sheet invariant I_z to the electron distribution function, although I_z may still be a valid adiabatic invariant for electrons.

[34] To complement the Ampère's equation and the quasi-neutrality equation within the current sheet, similar to the cases of the Harris model and the SGS model, a specific frame satisfying the condition $v_{Dic} T_{ec} + v_{Dec} T_{ic} = 0$ is selected, and an additional assumption of $v_{Diw} T_{ew} + v_{Dew} T_{\parallel iw} = 0$ is also made. It should be noted that these two conditions may become redundant in the presence of a background plasma population [Yoon and Lui, 2004; Sitnov *et al.*, 2006], however, as we limit our study to the cases with no background population, these two conditions remain crucial in the construction of the current sheet model.

[35] These two conditions further ensure that the electrostatic field outside the current sheet is zero in the specific frame, and the frame is called the stationary frame of the current sheet (which is similar to the deHoffmann-Teller frame but allows a nonzero intrinsic electric field along the normal direction, as was discussed by Khrabrov and Sonnerup [1998]).

[36] Given the parameter series of N_w , N_c , v_{Diw} , v_{Dic} , $T_{\parallel iw}$, $T_{\perp iw}$, T_{ic} , T_{ec} and T_{ew} , which can be also used to calculate the values of v_{Dec} and v_{Dew} on the basis of the two conditions discussed above, we are able to obtain the self-consistent profiles of the magnetic field and the plasma density, by numerically solving the Ampère's equation and the quasi-neutrality equation following the procedures similar to the ones described by Sitnov *et al.* [2003, 2004]. Maybe more importantly, the location-dependent ion and electron distributions within the entire current sheet, as the function of the velocity vectors, can also be obtained.

[37] The next step is to validate the modified SGS model, by performing a best fit procedure with the series of

unknown parameters, to compare with the ion distributions observed by P1. Before doing this, some additional parameters are introduced to place the satellite into the modeled current sheet, i.e., the distance of the satellite to the neutral sheet H , the tilt angle θ between the current sheet and the xy plane in the spacecraft coordinates, and the velocity of the satellite in the stationary frame of the current sheet.

[38] It should be noted that some of the parameters can be obtained directly from the observed ion and electron distributions. Although the parallel and perpendicular temperature of the warmer ion component cannot be directly obtained from the observation, all of the other three components (the colder component of ions, the colder and warmer components of electrons) are found to hold the simple shifted Maxwellian form, which is consistent with equation (9) and equation (10), with the thermal velocities of 280 km s⁻¹, 4700 km s⁻¹, and 21000 km s⁻¹, respectively. Their temperature, i.e., T_{ic} , T_{ec} and T_{ew} , is accordingly calculated to be 410 eV, 63 eV and 1.3 keV, respectively.

[39] Another parameter that can be obtained before performing the best fit procedure is the tilt angle θ . As can be derived from equation (9), the cut of the ion distribution in the plane perpendicular to the magnetic field should have an axis of symmetry, that is, the y axis of the modeled current sheet. In Figure 3a, the axis of symmetry can be found as the thick dashed line, with an angle of 20° with the y axis, which suggests that the current sheet was slightly tilted, by $\theta = 20^\circ$, from the xy plane of the spacecraft coordinates.

[40] Furthermore, the parameter series are subjected to some additional constraints. In the modeled current sheet, the magnetic field and the plasma density at the location of the satellite can be both expressed by the parameter series, which should be equal to the observed values of 15.5 nT and 0.55 cm⁻³, respectively. Moreover, the magnetic field outside the modeled current sheet, which can also be fully determined by the parameter series, should be equal to 18.8 nT which is calculated by assuming the pressure balance between the current sheet and the lobe region.

[41] The best fit procedure is then performed with these constraints, by minimizing the sum of the squared logarithmic differences between the observed and the modeled ion distributions in the yz plane. The parameter series are then calculated as follows: $N_w = 0.13$ cm⁻³, $N_c = 1.12$ cm⁻³, $v_{Diw} = 421$ km s⁻¹, $v_{Dic} = 25.2$ km s⁻¹, $T_{\parallel iw} = 1.88$ keV, $T_{\perp iw} = 3.86$ keV, and $H = 1260$ km. The stationary frame of the modeled current sheet is further estimated to be moving dawnward at a speed of 110 km s⁻¹ in the spacecraft coordinates. On the basis of the derived parameters, the necessary condition (6) for using I_z as the invariant of motion becomes $|B_z| \ll 12.6$ nT, which is well satisfied by the observed B_z of ~ 0.2 nT.

[42] Figures 4a and 4b are the yz cut and the xy cut of the modeled ion distribution with the parameters cited above, which reproduce most of the key features of the P1 observations (shown in Figures 3a and 3b), that is, the isotropic colder component and the nongyrotropic warmer component with more ions moving duskward.

[43] The nongyrotropy of the warmer ions partly arises from the fact that the diamagnetic drift velocity for the warmer ion component (v_{Diw}) is remarkably greater than that for the colder one (v_{Dic}), which systematically shifts the

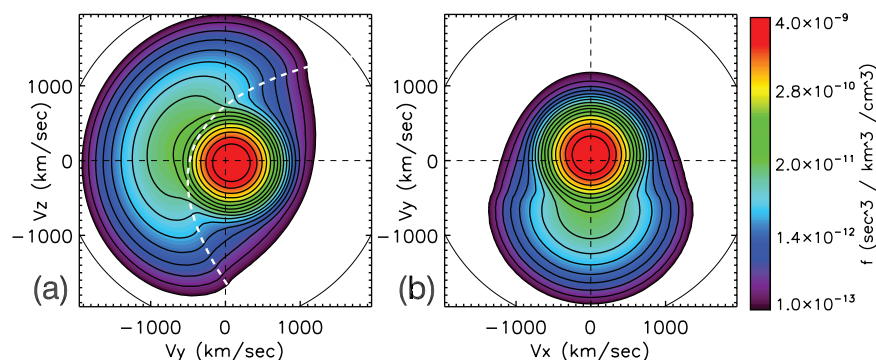


Figure 4. The ion distribution function of the modified SGS model, which is validated by a best fit procedure to match the P1 observational data shown in Figures 3a and 3b. (a) The cut of the distribution in the yz plane, in which the white dashed line separates the ions following the meandering orbits with those gyrating around the magnetic field. (b) The cut in the xy plane.

warmer ion component duskward in the velocity space. However, this effect alone would elongate the shape of the ion distribution in the dawn-dusk direction, but not in the north-south direction shown both in the observations (Figure 3a) and in the modeled current sheet (Figure 4a). To explain this phenomenon, the contribution of the sheet invariant I_z to the ion distribution function should be highlighted.

[44] The white dashed line in Figure 4a, calculated by the given parameter series of the modeled current sheet, suggests a boundary in the yz plane of the velocity space to separate the gyrating ions (to the right of the line) with those meandering across the neutral sheet. In the vicinity to the left of the dashed line, the I_z values are larger (located in the shaded area of Figure 1), and because of the positive contribution of the I_z to the distribution function (since $T_{\perp iw} > T_{\parallel iw}$), the phase space densities in this region would be enhanced. Those ions far away from the dashed line in the velocity space, on the other hand, correspond to

relatively lower values of I_z , which consequently decrease the phase space densities. As can be seen in Figure 4a, in the energy range of interest, the white dashed line is mainly in the north-south direction, therefore, the shape of the ion distribution is also elongated in the same direction.

[45] As a combination of the two effects described above, a mushroom-shaped structure of the ion distribution is formed in the plane perpendicular to the magnetic field, along with a density cavity in the rightmost region of the velocity space, which agrees with the observations very well.

[46] Besides its capability of reproducing the observed ion distributions, the model provides information about the current sheet. For example, the thickness of the current sheet can be evaluated by the distance of the satellite to the neutral sheet, which is estimated to be 1260 km. More precisely, the profile of the normalized magnetic field versus the distance to the neutral sheet is shown in Figure 5a as the solid line, and the heavy dot represents the location of the

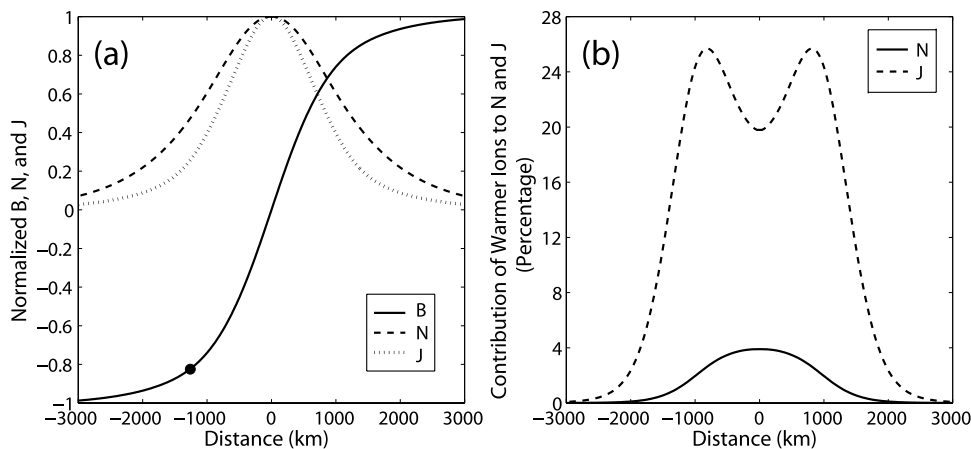


Figure 5. (a) The normalized profiles of the magnetic field (solid line), the plasma density (dashed line), and the electric current density (dotted line) within the modeled current sheet. The heavy dot represents the location of the satellite. (b) The percentage of the warmer ion density to the local plasma density (solid line) and the percentage of the electric current carried by the warmer ion component to the local current density (dashed line) at each location of the current sheet.

P1 satellite in the modeled current sheet. The characteristic thickness of the current sheet, if defined by the location with the magnetic field $\tanh(1) = 0.762$ times of the field outside the current sheet (similar to the definition of L in the Harris sheet), can be thus calculated to be 1050 km.

[47] Also shown in Figure 5a are the profiles of the plasma density and the current density in the current sheet, as the dashed and the dotted lines, respectively. The difference between these two profiles, although relatively small compared to the original SGS model and to some previous observations [e.g., *Runov et al.*, 2005], also highlights the deviation of the modeled current sheet from the standard Harris sheet, which arises from the I_z -dependent distribution function of the warmer ion component. Actually, if the warmer ion and electron components are removed from the system, the standard Harris profiles would appear with the current sheet thickness of $2cT_{ic}/eB_0v_{Dic} = 1730$ km, in comparison with 1050 km as was obtained from the model. In other words, the thickness of the current sheet can be significantly reduced by the existence of the warmer particles.

[48] Figure 5b shows the contribution of the warmer ion component to the plasma density and the current density at each location within the current sheet. The percentage of the warmer ion density to the local plasma density decreases, from $\sim 4\%$ to completely negligible, as the distance to the neutral sheet increases. That is to say, there exists a thinner layer of warmer ions embedded within the current sheet. The very sharp density gradient for warmer ions, therefore, suggests a strong asymmetry of the warmer ion distribution in the y direction due to the diamagnetic effect, which agrees with the greater value of $v_{D_{iw}}$ (the diamagnetic drift velocity of warmer ions) than that of v_{Dic} (the diamagnetic drift velocity of colder ions).

[49] As a consequence of its much larger diamagnetic drift velocity, the warmer ion component can carry a significant fraction ($\sim 25\%$) of the cross-tail current, despite its lower ($< 4\%$) density. Therefore, as is shown in Figure 5a, the current density profile can be even more concentrated in the center of the current sheet (than the plasma density profile), and the current sheet thickness becomes smaller.

[50] Because most of the warmer ions are experiencing meandering orbits across the neutral sheet, the role of the meandering ions in the nature of the current sheet should also be emphasized. Actually, the percentage of the electric current carried by warmer ions to the current density shows a bifurcated profile with a local minimum in the center of the current sheet, which is caused by the different I_z values between meandering and gyrating ions and the positive I_z contribution to the ion distribution function as discussed in section 2.

[51] It should be noted that there is an alternative explanation of the observed nongyrotropic distribution function, which is called the remote sensing effect [*Wilber et al.*, 2004; *Lee et al.*, 2004]. However, the physical essence of the remote sensing effect, that is, the phase space density dependence on gyrophase can be associated with the guiding center location difference and the spatial gradient of the plasma pressure [*Schwartz et al.*, 1998], is actually very similar to the diamagnetic effect suggested in our interpretation. The most remarkable difference between them is that the remote sensing effect relies on the guiding center

approximation, and can only qualitatively explain the origin of the nongyrotropy when the current sheet becomes thin enough to invalidate the guiding center theory. Our kinetic-based model, on the other hand, does not depend on the guiding center approximation. Therefore, the model can provide us more flexibility to quantitatively examine the structure of the current sheet (either thin or thick), and to differentiate the different roles of the meandering and gyrating particles.

5. Discussions

[52] As was discussed before and confirmed by particle simulations performed by *Sitnov et al.* [2006], the SGS current sheet is rather stable despite the greater number of possible wave modes due to the anisotropic and nongyrotropic distributions. It is also interesting to note that the anisotropy-driven mirror and firehose instabilities can be well diminished by the nongyrotropic features of the SGS model. However, our modification on the SGS model introduces the coexistence of warmer and colder ion components with different drift velocities, which may favor the excitation of the ion-ion kink instability [*Daughton*, 1999]. Although the stability analysis is not included in this paper, it should be kept in mind that instabilities can reorganize the current sheet structure and may further be related to the onset of the magnetic reconnection [e.g., *Motshmann and Glassmeier*, 1998; *Zelenyi et al.*, 2008].

[53] As magnetic reconnection continues, a negative B_z component should appear in the current sheet tailward of the reconnection site. Although the negative B_z component can hardly change the trajectories of the gyrating ions, those ions originally experiencing meandering orbits, as was suggested by *Speiser* [1965], would be turned toward the tail during their duskward motion and eventually be ejected from the current sheet.

[54] The evolution of the ion distribution observed by P1, which was located tailward of the reconnection site and southward of the neutral sheet, is shown in Figure 6. Here Figures 6a and 6b correspond to the time interval 15 s and 30 s later than that of Figure 3b. During these time periods, the observed B_z component in the GSM coordinate system are -1.1 nT and -2.5 nT, respectively, in comparison with the previous B_z value of 0.2 nT.

[55] The distribution of colder ions, most of which experience gyrating orbits and therefore cannot access the neutral sheet, shows very small changes with the distribution displayed in Figure 3b. The warmer ions, especially those meandering duskward, on the other hand, increasingly show tailward motions which suggest the appearance of the negative B_z component in the current sheet.

[56] However, it should be noted that the current sheet model we use in the paper is unable to reproduce these ion distributions. The three invariants of motion used in the model (W , P_y and I_z) are either even functions of v_x or independent on v_x , and therefore the modeled distribution functions can only be even functions of v_x , which cannot provide the asymmetry shown in Figures 6a and 6b. The introduction of another invariant, the x component of the canonical momentum P_x in the presence of B_z and the y -dependent A_x , may be helpful to solve the problem and therefore provide a more flexible current sheet model.

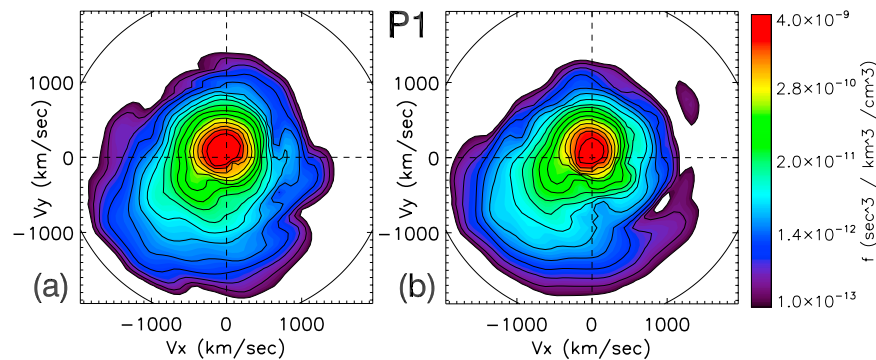


Figure 6. THEMIS P1 observations of the ion distribution functions in the xy plane, with the same format as Figure 3b. The time intervals selected are (a) 0450:32–0450:41 UT and (b) 0450:47–0450:56 UT.

However, the topic is beyond the scope of this paper, and is planned to be addressed in our future studies.

6. Summary

[57] By studying the THEMIS observations, we have clearly shown that the ions in the tail current sheet are nongyrotropic during the substorm late growth phase, which significantly deviates from the standard *Harris* [1962] model. By taking into account the quasi-adiabatic properties of the ion meandering motion in the distribution function, the current sheet model with nongyrotropic features can be established, as was suggested by *Sitnov et al.* [2003, 2004, 2006]. The SGS model is slightly modified in this paper, to consider both the colder and the warmer ion components, and the modified model is validated by a best fit procedure to compare with the observational data. Most of the key signatures of the observed ion distribution are able to be reproduced by the model. Both the strong diamagnetic drift velocity of the warmer ion component and the meandering motion of these ions are found to play important roles in producing the nongyrotropic feature of the ion distribution, and to reorganize the structure of the thin current sheet.

[58] **Acknowledgments.** The work was supported by NASA grant NAS5-02099. The authors are truly grateful to M. G. Kivelson, M. Ashour-Abdalla, V. A. Sergeev, H. Zhang, Y. S. Ge, and A. Keiling for helpful discussions. Special thanks to A. Prentice for polishing the English syntax of this paper.

[59] Wolfgang Baumjohann thanks the reviewers for their assistance in evaluating this paper.

References

- Angelopoulos, V. (2008), The THEMIS mission, *Space Sci. Rev.*, *141*, 5–34, doi:10.1007/s11214-008-9336-1.
- Angelopoulos, V., et al. (2008), Tail reconnection triggering substorm onset, *Science*, *321*, 931–935, doi:10.1126/science.1160495.
- Asano, Y., T. Mukai, M. Hoshino, Y. Saito, H. Hayakawa, and T. Nagai (2004), Statistical study of thin current sheet evolution around substorm onset, *J. Geophys. Res.*, *109*, A05213, doi:10.1029/2004JA010413.
- Asano, Y., R. Nakamura, W. Baumjohann, A. Runov, Z. Vörös, M. Volwerk, T. L. Zhang, A. Balogh, B. Klecker, and H. Rème (2005), How typical are atypical current sheets?, *Geophys. Res. Lett.*, *32*, L03108, doi:10.1029/2004GL021834.
- Auster, H. U., et al. (2008), The THEMIS Fluxgate Magnetometer, *Space Sci. Rev.*, *141*, 235–264, doi:10.1007/s11214-008-9365-9.
- Baumjohann, W., et al. (2007), Dynamics of thin current sheets: Cluster observations, *Ann. Geophys.*, *25*, 1365–1389.
- Birn, J., and E. R. Priest (2007), *Reconnection of Magnetic Fields: Magnetohydrodynamics and Collisionless Theory and Observations*, Cambridge Univ. Press, Cambridge, U.K.
- Birn, J., K. Schindler, and M. Hesse (2004), Thin electron current sheets and their relation to auroral potentials, *J. Geophys. Res.*, *109*, A02217, doi:10.1029/2003JA010303.
- Büchner, J., and L. M. Zelenyi (1989), Regular and chaotic charged particle motion in magnetotail-like field reversals: 1. Basic theory of trapped motion, *J. Geophys. Res.*, *94*, 11,821–11,842.
- Camporeale, E., and G. Lapenta (2005), Model of bifurcated current sheets in the Earth's magnetotail: Equilibrium and stability, *J. Geophys. Res.*, *110*, A07206, doi:10.1029/2004JA010779.
- Channell, P. J. (1976), Exact Vlasov-Maxwell equilibria with sheared magnetic fields, *Phys. Fluids*, *19*, 1541–1545.
- Cowley, S. W. H. (1978), The effect of pressure anisotropy on the equilibrium structure of magnetic current sheets, *Planet. Space Sci.*, *26*, 1037–1061, doi:10.1016/0032-0633(78)90028-4.
- Daughton, W. (1999), The unstable eigenmodes of a neutral sheet, *Phys. Plasmas*, *6*, 1329–1343, doi:10.1063/1.873374.
- Francfort, P., and R. Pellat (1976), Magnetic merging in collisionless plasmas, *Geophys. Res. Lett.*, *3*, 433–436.
- Génot, V., F. Mottez, G. Fruit, P. Louam, J.-A. Sauvaud, and A. Balogh (2005), Bifurcated current sheet: Model and Cluster observations, *Planet. Space Sci.*, *53*, 229–235, doi:10.1016/j.pss.2004.09.048.
- Harris, E. G. (1962), On a plasma sheath separating regions of oppositely directed magnetic field, *Nuovo Cimento*, *23*, 115–121.
- Hoshino, M., T. Mukai, T. Yamamoto, and S. Kokubun (1998), Ion dynamics in magnetic reconnection: Comparison between numerical simulation and Geotail observations, *J. Geophys. Res.*, *103*, 4509–4530, doi:10.1029/97JA01785.
- Khrabrov, B. V., and B. U. Ö. Sonnerup (1998), Dehoffmann-teller analysis, in *Analysis Methods for Multi-Spacecraft Data*, edited by G. Paschmann and P. Daly, pp. 221–248, Eur. Space Agency, Noordwijk, Netherlands.
- Kropotkin, A. P., H. V. Malova, and M. I. Sitnov (1997), Self-consistent structure of a thin anisotropic current sheet, *J. Geophys. Res.*, *102*, 22,099–22,032, doi:10.1029/97JA01316.
- Lee, E., M. Wilber, G. K. Parks, K. W. Min, and D.-Y. Lee (2004), Modeling of remote sensing of thin current sheet, *Geophys. Res. Lett.*, *31*, L21806, doi:10.1029/2004GL020331.
- Lembège, B., and R. Pellat (1982), Stability of a thick two-dimensional quasineutral sheet, *Phys. Fluids*, *25*, 1995–2004.
- McFadden, J. P., C. W. Carlson, D. Larson, V. Angelopoulos, M. Ludlam, R. Abiad, B. Elliott, P. Turin, and M. Marckwardt (2008), The THEMIS ESA plasma instrument and in-flight calibration, *Space Sci. Rev.*, *141*, 277–302.
- Mitchell, D. G., D. J. Williams, C. Y. Huang, L. A. Frank, and C. T. Russell (1990), Current carriers in the near-Earth cross-tail current sheet during substorm growth phase, *Geophys. Res. Lett.*, *17*, 583–586.
- Motschmann, U., and K. H. Glassmeier (1998), Relation of magnetic field line reconnection and unstable nongyrotropic particle distributions, in *Substorms-4, Astrophys. and Space Sci. Libr.*, vol. 238, edited by S. Kokubun and Y. Kamide, pp. 491–496, Terra Sci., Tokyo.
- Mottez, F. (2003), Exact nonlinear analytic Vlasov-Maxwell tangential equilibria with arbitrary density and temperature profiles, *Phys. Plasmas*, *10*, 2501–2508, doi:10.1063/1.1573639.
- Runov, A., R. Nakamura, W. Baumjohann, T. L. Zhang, M. Volwerk, H.-U. Eichelberger, and A. Balogh (2003), Cluster observation of a bifurcated current sheet, *Geophys. Res. Lett.*, *30*(2), 1036, doi:10.1029/2002GL016136.
- Runov, A., et al. (2005), Electric current and magnetic field geometry in flapping magnetotail current sheets, *Ann. Geophys.*, *23*(4), 1391–1403.

- Runov, A., et al. (2008), Observations of an active thin current sheet, *J. Geophys. Res.*, *113*, A07S27, doi:10.1029/2007JA012685.
- Schindler, K. (1972), A self-consistent theory of the tail of the magnetosphere, in *Earth's Magnetospheric Processes, Astrophys. and Space Sci. Libr.*, vol. 32, edited by B. M. McCormac, pp. 200–206, D. Reidel, Dordrecht, Netherlands.
- Schindler, K., and J. Birn (2002), Models of two-dimensional embedded thin current sheets from Vlasov theory, *J. Geophys. Res.*, *107*(A8), 1193, doi:10.1029/2001JA000304.
- Schwartz, S. J., P. W. Daly, and A. N. Fazakerley (1998), Multi-spacecraft analysis of plasma kinetics, in *Analysis Methods for Multi-Spacecraft Data*, edited by G. Paschmann and P. W. Daly, pp. 159–184, Eur. Space Agency, Bern, Switzerland.
- Sergeev, V. A., D. G. Mitchell, C. T. Russell, and D. J. Williams (1993), Structure of the tail plasma/current sheet at 11 Re and its changes in the course of a substorm, *J. Geophys. Res.*, *98*, 17,345–17,366, doi:10.1029/93JA01151.
- Sitnov, M. I., P. N. Guzdar, and M. Swisdak (2003), A model of the bifurcated current sheet, *Geophys. Res. Lett.*, *30*(13), 1712, doi:10.1029/2003GL017218.
- Sitnov, M. I., M. Swisdak, J. F. Drake, P. N. Guzdar, and B. N. Rogers (2004), A model of the bifurcated current sheet: 2. Flapping motions, *Geophys. Res. Lett.*, *31*, L09805, doi:10.1029/2004GL019473.
- Sitnov, M. I., M. Swisdak, P. N. Guzdar, and A. Runov (2006), Structure and dynamics of a new class of thin current sheets, *J. Geophys. Res.*, *111*, A08204, doi:10.1029/2005JA011517.
- Sonnerup, B. U. O. (1971), Adiabatic particle orbits in a magnetic null sheet, *J. Geophys. Res.*, *76*, 8211–8222.
- Speiser, T. W. (1965), Particle trajectories in model current sheet: 1. Analytic solution, *J. Geophys. Res.*, *70*, 4219–4226.
- Wilber, M., et al. (2004), Cluster observations of velocity space-restricted ion distributions near the plasma sheet, *Geophys. Res. Lett.*, *31*, L24802, doi:10.1029/2004GL020265.
- Yoon, P. H., and A. T. Y. Lui (2004), Model of ion- or electron-dominated current sheet, *J. Geophys. Res.*, *109*, A11213, doi:10.1029/2004JA010555.
- Zelenyi, L. M., M. I. Sitnov, H. V. Malova, and A. S. Sharma (2000), Thin and superthin ion current sheets: Quasi-adiabatic and nonadiabatic models, *Nonlinear Processes Geophys.*, *7*, 127–139.
- Zelenyi, L., A. Artemiev, H. Malova, and V. Popov (2008), Marginal stability of thin current sheets in the Earth's magnetotail, *J. Atmos. Sol. Terr. Phys.*, *70*, 325–333.
- Zhou, X.-Z., Z. Y. Pu, Q.-G. Zong, and L. Xie (2007), Energy filter effect for solar wind particle entry to the plasma sheet via flank regions during southward interplanetary magnetic field, *J. Geophys. Res.*, *112*, A06233, doi:10.1029/2006JA012180.

V. Angelopoulos, A. Runov, and X.-Z. Zhou, Institute of Geophysics and Planetary Physics, University of California, Los Angeles, CA 90095, USA. (xzhou@igpp.ucla.edu)

F. Coroniti and P. Pritchett, Department of Physics and Astronomy, University of California, Los Angeles, CA 90095, USA.

K.-H. Glassmeier, Institute for Geophysics and Extraterrestrial Physics, TU Braunschweig, D-38106 Braunschweig, Germany.

D. Larson and J. P. McFadden, Space Science Laboratory, University of California, Berkeley, CA 94720, USA.

Z. Y. Pu and Q.-G. Zong, School of Earth and Space Sciences, Peking University, Beijing 100871, China.

M. I. Sitnov, Johns Hopkins University Applied Physics Laboratory, Laurel, MD 20723, USA.